

Abstract

We present a seismic attenuation model for the crust beneath the Cenozoic basaltic field of Lunayyir (western Saudi Arabia), where a strong seismic swarm occurred in 2009. The tomography inversion uses the envelope shape of the *S* wave seismograms from over 300 strong events ($M > 3.5$). The resulting attenuation structures appear to be consistent with the distribution of seismic velocities. The obtained 3-D attenuation model distinguishes the low-attenuation zones down to 5 km depth corresponding to the rigid basaltic cover. At greater depths, we detect a high-attenuation anomaly coinciding with the main seismicity cluster. We propose that this zone corresponds to the upper part of the conduit area ascending from deeper magma sources. According to the distributions of local events, fluids and melts from this conduit appear to reach a depth of ~ 2 km, but were not able to reach the surface and cause the eruption in 2009.

1 Introduction

The western part of the Arabian Peninsula is characterized by a wide distribution of Cenozoic basaltic fields (harrats). Some of these fields are still active and present a real eruption potential. During the human history time there were several records of eruptions occurred within the harrats of Saudi Arabia and Yemen (e.g., Camp et al., 1987). The harrats are located close to the western coast of the Arabian Peninsula, and their appearance is thought to be linked to the rifting of the Red Sea (e.g., Cochran and Martinez, 1988). However, the role that the opening of the Red Sea played in the origination of Lunayyir and other harrats appears to be rather complex. Unlike the southern Red Sea segment, which has a clear ocean-type spreading, the extension of the northern segment appears to result from the stretching of the continental crust at a rate of ~ 10 mm year⁻¹ (Cochran and Karner, 2007). According to regional tomography studies (e.g., Chang et al., 2011), no low-velocity anomalies, which could be associated

SED

6, 1401–1421, 2014

Attenuation structure beneath Harrat Lunayyir

I. Koulakov et al.

Title Page

Abstract

Introduction

Conclusions

References

Tables

Figures



Back

Close

Full Screen / Esc

Printer-friendly Version

Interactive Discussion



**Attenuation structure
beneath Harrat
Lunayyir**

I. Koulakov et al.

Title Page

Abstract

Introduction

Conclusions

References

Tables

Figures



Back

Close

Full Screen / Esc

Printer-friendly Version

Interactive Discussion



with hot areas, have been observed beneath the Red Sea. Instead, negative seismic anomalies align beneath the western part of the Arabian plate exactly where the volcanic fields are located. These observations may give arguments for the passive character of rifting in the Northern Red Sea. However the lithosphere extension may cause the asthenosphere upwelling beneath the coastal areas that is responsible for the volcanic activity.

Lunayyir is one of the youngest harrats in Saudi Arabia (less than 1 Ma, Pallister et al., 2010), and it is small relative to other Cenozoic basaltic fields in the Arabian Peninsula. In Lunayyir, recent basalts cover an area that is over 3500 km² in size (Fig. 1b). The last eruption in this area occurred approximately 1000 years ago (Camp et al., 1987); however, elevated groundwater temperatures and the existence of fumaroles indicate that strong thermal activities still occur in this zone (e.g., Al-Dayel, 1988). This volcanic field is considered a probable candidate for the next eruption. Before 2009, weak to moderate seismicity mostly associated with tectonic crustal displacements in the Red Sea and Gulf of Aqaba was observed in this area (e.g., El-Isa and Al-Shanti, 1989; Al-Amri, 1995). In April–July 2009, a strong swarm of over 30 000 earthquakes reaching a magnitude of 5.4 occurred in the Lunayyir area. Most of these events were confined to have been oriented along a NNW–SSE line that was approximately 20 km long in the northern part of the Harrat (Fig. 1b). This seismicity included both high- and low-frequency events (Pallister et al., 2010) that might indicate the potential volcanic nature of this swarm. This hypothesis was supported by models based on InSAR and geodetic data developed by Baer and Hamiel (2010) who proposed a vertical dyke intrusion.

Questions relating to the origin of this swarm and the possible continuation of these processes lead to vital discussions in the scientific community. Studying the deep structure beneath the Lunayyir area can greatly help with understanding these problems. The spatial and temporal distributions of the seismicity and earthquake mechanisms were carefully studied by Zobin et al. (2013). They compared the main seismic activity features to several volcanoes around the world and concluded that a further volcanic

and Lindley, 1994), Etna (Martínez-Arévalo et al., 2005), Central Andes (Shurr et al., 2003; Koulakov et al., 2006), and Kilauea (Hansen et al., 2004). Most of these studies used a technique based on retrieving t^* by analyzing P wave arrivals. The t^* values of the S waves at different frequencies were used in some studies, such as the tomographic inversion of the North-Anatolian fault (Koulakov et al., 2010). A similar approach was used in the present study; however, instead of using t^* , we estimated the attenuation parameter by analyzing the envelope shape of the S wave signal, as proposed in the classic work by Aki and Chouet (1975). In this study, we provide the seismic attenuation distribution beneath the Lunayyir area, which helps us understand the origin of recent seismic activities.

2 Data and algorithms

After the beginning of the seismic crisis in April 2009, a seismic network was installed in the Lunayyir area by the King Abdulaziz City of Science and Technology (KACST), King Saud University (KSU), and the Saudi Geological Survey (SGS). Data for over 5700 events using autopicked P arrival times were used by Hansen et al. (2013). In this study, we manually re-analyzed the same waveform data. We selected 1879 strong events with the magnitudes above 3.2 and identified 8904 P and 10579 S phases for most of these events at the available stations, which enabled the robust locating of the sources. It is interesting there were slightly more S phases than P phases, which can be explained by the clearer and stronger S wave signal. These data were used to run a simultaneous tomographic inversion for P and S velocities and source locations based on the iterative LOTOS algorithms (Koulakov, 2009). The results of the velocity inversion are described in details in (Koulakov et al., 2014). The resulting velocity model, which is presented in Fig. 2, is used in this study as the background model for the attenuation tomography.

After performing the source locations, we analyzed the seismograms of every source–receiver pair to estimate the attenuation parameters of each ray. We used

SED

6, 1401–1421, 2014

Attenuation structure beneath Harrat Lunayyir

I. Koulakov et al.

Title Page

Abstract

Introduction

Conclusions

References

Tables

Figures

⏪

⏩

◀

▶

Back

Close

Full Screen / Esc

Printer-friendly Version

Interactive Discussion



Attenuation structure beneath Harrat Lunayyir

I. Koulakov et al.

Title Page

Abstract

Introduction

Conclusions

References

Tables

Figures

⏪

⏩

◀

▶

Back

Close

Full Screen / Esc

Printer-friendly Version

Interactive Discussion



the basic attenuation estimation principles proposed in the classic work of Aki and Chouet (1975). The physical background of the method is schematically illustrated in Fig. 3. We are studying the intrinsic attenuation, which is responsible for conversion of a part of the seismic energy into the heat and leads to the decrease of the amplitude of seismic signal on the seismogram. However direct deriving the attenuation values from measurement of the amplitude of seismic signal is an ambiguous task, because the amplitude may be also affected by a variety of different factors, such as source characteristics, geometrical spreading, focusing/defocusing, scattering, reflections etc. Studying the properties of seismic signal following the main wave arrival (seismic coda) provides more information on the medium intrinsic attenuation. For example, striking a piece of metal with low attenuation yields a sound that is affected by the existence of numerous scatterers and reflectors that can be heard for a rather long time (long flat coda). Alternatively, sound from a highly attenuated wooden balk would be much shorter (short coda). When studying the earth structures, it is presumed that the medium contains a large amount of scatters which are more or less uniformly distributed throughout the space (hatches in Fig. 3). In this case, besides the direct wave there are infinite number of secondary scattering waves which compose the coda. The properties of the coda depend on the properties of the medium in which the main and scattered waves propagate. In case of highly attenuated medium (e.g., corresponding to station B in Fig. 3) more energy of the seismic waves will be converted into the heat and this causes stronger decay of the envelop amplitude compared to the direct wave. For the low-attenuation medium (case of station A) the coda decrement is longer. Aki and Chouet (1975) approximated the envelope for seismic code after the arrival of the main wave using an exponential dependence:

$$A(f, t) = t^{-\beta} A_0 \exp\left(\frac{-\pi f t}{Q(f)}\right) \quad (1)$$

where t is travel time, A_0 is the signal amplitude in the source area, f is its frequency, and $Q(f)$ is a quality factor (inverse of the attenuation). Figure 4a shows a real seismogram corresponding to the horizontal component filtered at 3 Hz. The envelope of the

waveform is shown in Fig. 4b. Applying a logarithmic transformation and then smoothing (central moving average in a 2 s interval) provides the curve shown in Fig. 4c, which can be approximated using a straight line directly associated to the attenuation:

$$\ln(A(f, t)) + \beta \ln(t) = \ln(A_0) - \frac{-\pi f t}{Q(f)} \quad (2)$$

5 The effect of geometrical spreading can be easily estimated using existing seismic ray parameters in the existing velocity model. Thus, the slope of the fit line shown in Fig. 4c is proportional to the attenuation value, $1/Q$. For example, a gentle slope (long code) indicates a high-quality factor and low attenuation. To avoid small numbers in the output from the tomography inversion, we use the inverse of the attenuation multiplied by 1000. Because of the uncertainty in A_0 , we cannot obtain an absolute value for the quality factor. Therefore, we use the average estimated values as a reference for the quality factor. We computed the relative positive and negative deviations in the quality factor for the inversion with respect to the reference value.

15 In the analysis of seismograms, we consider a 10 s lapse window starting at 1 s after the arrival of the S phase. This is different of a common way for computing the slope of the Q coda which is usually based on the two travel times of the S wave as a starting point (e.g., Aki, 1980; Rautian and Khalturin, 1979). We could not use the traditional definition of coda because for most events the signal was not very strong. After the moment of two S travel times, the low signal/noise ratio made the determinations of the coda characteristics very unstable. The delay of 1 s seems to us optimal to start the lapse window as corresponding to the maximum amplitude of the direct waves. Just after the first arrival, the shape of the seismogram is dependent on the source properties and usually not reaches the maximum immediately. In our experience, the best exponential approximation for the coda decrement can be obtained for
20 the window starting close to the moment of maximum of the direct wave. Comparing the amplitudes of direct and secondary waves seems to be more stable than the analysis of only secondary waves, which are strongly affected by many different factors (such

**Attenuation structure
beneath Harrat
Lunayyir**

I. Koulakov et al.

Title Page

Abstract

Introduction

Conclusions

References

Tables

Figures



Back

Close

Full Screen / Esc

Printer-friendly Version

Interactive Discussion



as distribution of scatters). We made several attempts of using other criteria for defining the start of the lapse times (such as two S times) but obtained unstable solutions which were inconsistent for different frequencies. In this sense, here we implement not commonly used estimate for slope of the Q coda, but the measurement of how large is the S wave packet compared to the coda waves (see for a wide discussion about this topic in Sato and Fehler, 1998; Gusev and Abubakirov, 1999). In other word, this Q coda parameter matches more to the measure of the S wave envelope broadening than directly to the estimation of the attenuation parameter along the ray path.

The data were independently processed across narrow-band-filtered seismograms with six different frequencies: 0.75, 1.50, 3, 6, 12 and 24 Hz. The processing results were carefully visually inspected for each ray. As a result, many data were rejected for not providing a clear linear approximation; only 4326 values had a sufficiently high quality for the inversion.

The attenuation tomographic inversion algorithm was generally identical to the first iteration step of the LOTOS code (Koulakov, 2009), which was initially designed for travel time passive source tomography. In our case, the source locations were obtained at a previous step of velocity tomography and remained unchanged when computing the attenuation. The rays were constructed using a bending ray tracer in the previously constructed 3-D S velocity model based on the travel time tomography (same as shown in Fig. 2). Note that the velocity model may affect the locations of sources. However, we performed the attenuation reconstructions using different velocity models and found that changes in the velocity model have minor effect upon the computed attenuation models. In this sense, the attenuation results appear to be completely independent on the 3-D velocity models. The ray coverage was used to construct a parameterization grid with nodes distributed according to the data density. The horizontal grid spacing was 2 km; in the vertical direction, the distances between nodes depended on the ray coverage and were not smaller than 0.5 km. Between the nodes, the velocity was linearly interpolated. To reduce the grid dependency of the results, we performed the inversion for four grids with different basic orientations and then average the com-

SED

6, 1401–1421, 2014

Attenuation structure beneath Harrat Lunayyir

I. Koulakov et al.

Title Page

Abstract

Introduction

Conclusions

References

Tables

Figures



Back

Close

Full Screen / Esc

Printer-friendly Version

Interactive Discussion



SED

6, 1401–1421, 2014

Attenuation structure beneath Harrat Lunayyir

I. Koulakov et al.

Title Page

Abstract

Introduction

Conclusions

References

Tables

Figures



Back

Close

Full Screen / Esc

Printer-friendly Version

Interactive Discussion



the solid basaltic rocks. The presence of some seismicity in this low-attenuation layer above the transition boundary indicates that the pressure in the conduit zone produced cracks in the upper layer but was insufficient to fracture the layer to the surface. It can be seen that the seismicity stopped at an approximate depth of 2 km. It may be speculated that the rigid cover prevented a new eruption in the Harrat Lunayyir. However, the facts all indicate the magma sources are still active and that these sources may find a weaker part of the crust in the future to create a conduit to the surface.

4 Conclusions

We constructed a 3-D model of the seismic attenuation distribution in the crust beneath the Harrat Lunayyir. Although less attenuation data were used compared to the travel time data used by Hansen et al. (2013), we achieved a sufficient resolution thanks to the absence of typical trade-offs between the source and model parameters existing for passive source travel time tomography.

The derived model clearly links to the observed geological features and allows the interpretation for the recent seismicity crisis in the Harrat Lunayyir. In the shallow layers, we identified the contrast between the low-attenuation layer within the basalt field and the high-attenuation zones in the surrounding the sedimentary basins. Below 6 km, we found a prominent high-attenuation zone that perfectly confines the narrow seismicity cluster observed in 2009. We propose that this high-attenuation pattern represents the upper portion of a conduit bringing fluids and/or melts from deep sources. Based on the derived attenuation model and seismicity distribution analyses, we conclude that this conduit most likely reached the depth of 6 km corresponding to the bottom of a rigid layer which is composed of basalts erupted during previous eruptions. The elevated pressure caused by the conduit process might create cracks within the rigid layer; however, it was insufficient to fracture fully to the surface. In this sense, this basaltic lid saved the area from a new eruption that may occur if the conduit discovers a weaker part of the crust to ascend.

Attenuation structure beneath Harrat Lunayyir

I. Koulakov et al.

Title Page

Abstract

Introduction

Conclusions

References

Tables

Figures



Back

Close

Full Screen / Esc

Printer-friendly Version

Interactive Discussion



- Cochran, J. and Martinez, F.: Structure and tectonics of the northern Red Sea: catching a continental margin between rifting and drifting, *Tectonophysics*, 150, 1–32, 1988.
- Cochran, J. R. and Karner, G. D.: Constraints on the deformation and rupturing of continental lithosphere of the Red Sea, in: *Imaging, Mapping, and Modeling Continental Lithosphere Extension and Breakup*, edited by: Karner, G. D. et al., *Geol. Soc. Publ.*, 282, 265–289, 2007.
- El-Isa, Z. H. and Al-Shanti, A.: Seismicity and tectonics of the Red Sea and western Arabia, *Geophys. J.*, 97, 449–457, 1989.
- Evans, J. R. and Zucca, J. J.: Active high-resolution seismic tomography of compressional wave velocity and attenuation structure at Medicine Lake Volcano, Northern California Cascade Range, *J. Geophys. Res.*, 93, 15016–15036, 1988.
- Gusev, A. A. and Abubakirov, I. R.: Vertical profile of effective turbidity reconstructed from broadening of incoherent body wave pulses – I. General approach and the inversion procedure, *Geophys. J. Int.*, 136, 295–308, 1999.
- Hansen, S., Thurber, C., Mandernach, M., Haslinger, F., and Doran, C.: Seismic velocity and attenuation structure of the east rift zone and south flank of Kilauea Volcano, Hawaii, *B. Seismol. Soc. Am.*, 94, 1430–1440, 2004.
- Hansen, S. E., DeShon, H. R., Moore-Driskell, M. M., and Al-Amri, A.: Investigating the *P* wave velocity structure beneath Harrat Lunayyir, northwestern Saudi Arabia, using double-difference tomography and earthquakes from the 2009 seismic swarm, *J. Geophys. Res.-Sol. Ea.*, 118, 4814–4826, 2013.
- Koulakov I.: LOTOS code for local earthquake tomographic inversion. Benchmarks for testing tomographic algorithms, *B. Seismol. Soc. Am.*, 99, 194–214, 2009.
- Koulakov, I., Sobolev S. V., and Asch G.: *P* and *S* velocity images of the lithosphere-aesthenosphere system in the Central Andes from local-source tomographic inversion, *Geophys. J. Int.*, 167, 106–126, 2006.
- Koulakov, I., Bindi, D., Parolai, S., Grosser, H., and Milkereit, C.: Distribution of seismic velocities and attenuation in the crust beneath the North Anatolian Fault (Turkey) from local earthquake tomography, *B. Seismol. Soc. Am.*, 100, 207–224, 2010.
- Koulakov, I., El Khrepy, S., Al-Arifi, N., Kuznetsov, P., and Kasatkina, E.: Images of the active magma sources beneath the Lunayyir basaltic field (Saudi Arabia) from local earthquake seismic tomography, *Earth Planet. Sc. Lett.*, in consideration, 2014.

Attenuation structure beneath Harrat Lunayyir

I. Koulakov et al.

[Title Page](#)
[Abstract](#)
[Introduction](#)
[Conclusions](#)
[References](#)
[Tables](#)
[Figures](#)




[Back](#)
[Close](#)
[Full Screen / Esc](#)
[Printer-friendly Version](#)
[Interactive Discussion](#)


- Lees, J. M. and Lindley, G. T.: Three-dimensional attenuation tomography at Loma Prieta: inversion of t^* for Q , *J. Geophys. Res.*, 99, 6843–6863, 1994.
- Martínez-Arévalo, C., Patanè, D., Rietbrock, A., and Ibáñez, J. M.: The intrusive process leading to the Mt. Etna 2001 flank eruption: constraints from 3-D attenuation tomography, *Geophys. Res. Lett.*, 32, L21309, 2005.
- Paige, C. C. and Saunders, M. A.: LSQR: an algorithm for sparse linear equations and sparse least squares, *ACM T. Math. Software*, 8, 43–71, 1982.
- Pallister, J. S., McCausl, W. A., Jónsson, S., Lu Z. H. M., El Hadidy, S., Aburukbah, A., Stewart, I. C. F., Lundgren, P. R., White, R. A., and Moufti, M. R. H.: Broad accommodation of rift-related extension recorded by dyke intrusion in Saudi Arabia, *Nat. Geosci.*, 3, 705–712, 2010.
- Rautian, T. G. and Khalturin, V. I.: The use of the coda for determination of the earthquake source spectrum, *B. Seismol. Soc. Am.*, 68, 923–948, 1978.
- Sato, H. and Fehler, M. C.: *Seismic Wave Propagation and Scattering in the Heterogeneous Earth*, AIP, New York, 308 pp., 1998.
- Schurr, B., Asch, G., Rietbrock, A., Trumbull, R., and Haberland, C. H.: Complex patterns of fluid and melt transport in the central Andean subduction zone revealed by attenuation tomography, *Earth Planet. Sc. Lett.*, 215, 105–119, 2003.
- Zobin, V. M., Al-Amri, A. M., and Fnais, M.: Seismicity associated with active, new-born, and re-awakening basaltic volcanoes: case review and the possible scenarios for the Harrat volcanic provinces, Saudi Arabia, *Arabian Journal of Geosciences*, 6, 529–541, 2013.

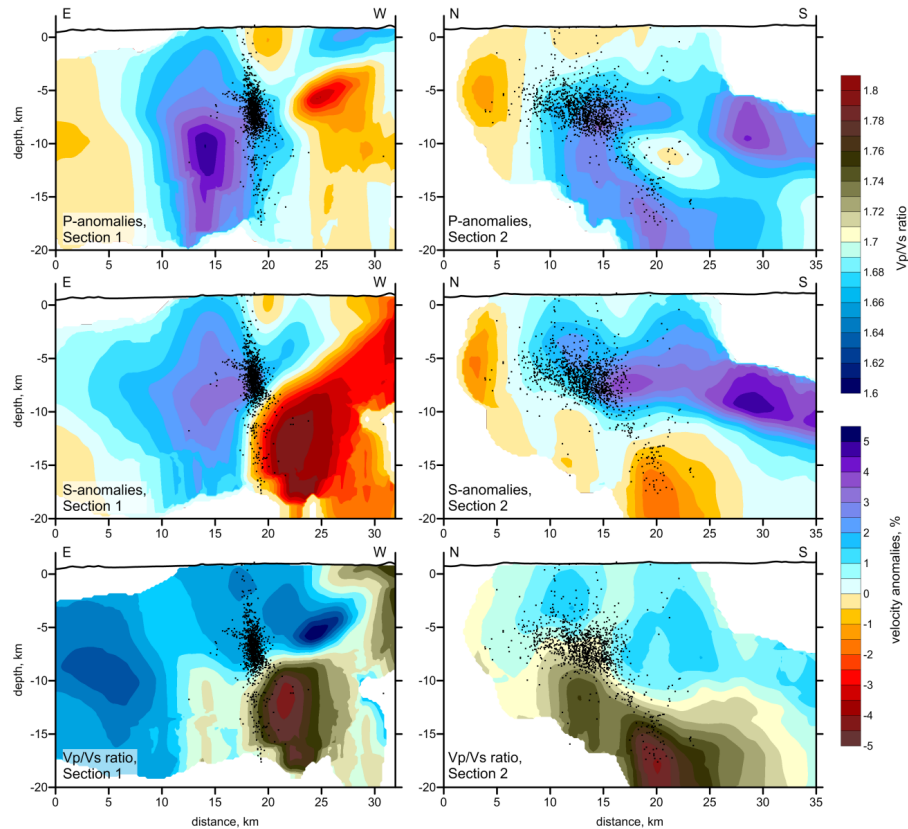


Figure 2. Velocity model (P , S anomalies and V_p/V_s ratio) and local source hypocenters (black dots) from Koulakov et al. (2014) in two vertical sections with the same locations as shown in Fig. 7. This model and source coordinates were used to construct the rays for the attenuation tomography in this study.

**Attenuation structure
beneath Harrat
Lunayyir**

I. Koulakov et al.

Title Page

Abstract

Introduction

Conclusions

References

Tables

Figures

◀

▶

◀

▶

Back

Close

Full Screen / Esc

Printer-friendly Version

Interactive Discussion



Attenuation structure beneath Harrat Lunayyir

I. Koulakov et al.

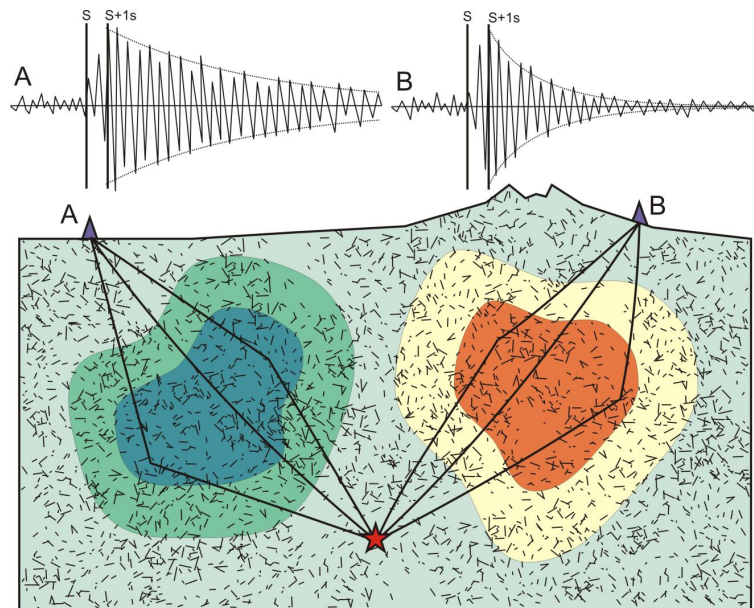


Figure 3. Schematic representation of the basic principle used for the attenuation inversion in this study. Hatches are the scatters which are roughly uniformly distributed within the study area. Red and blue indicate zones of high and low attenuation, respectively. Star is a source; triangles are the receivers; black lines are the direct and scattered rays between source and receivers. Above: schematic seismograms recorded at stations A and B corresponding to low and high attenuation areas. Dotted lines are the envelopes of the seismograms. Lines indicated with S and $S + 1\text{ s}$ mark the arrival time of the S wave and 1 s later point.

Title Page

Abstract

Introduction

Conclusions

References

Tables

Figures

◀

▶

◀

▶

Back

Close

Full Screen / Esc

Printer-friendly Version

Interactive Discussion



**Attenuation structure
beneath Harrat
Lunayyir**

I. Koulakov et al.

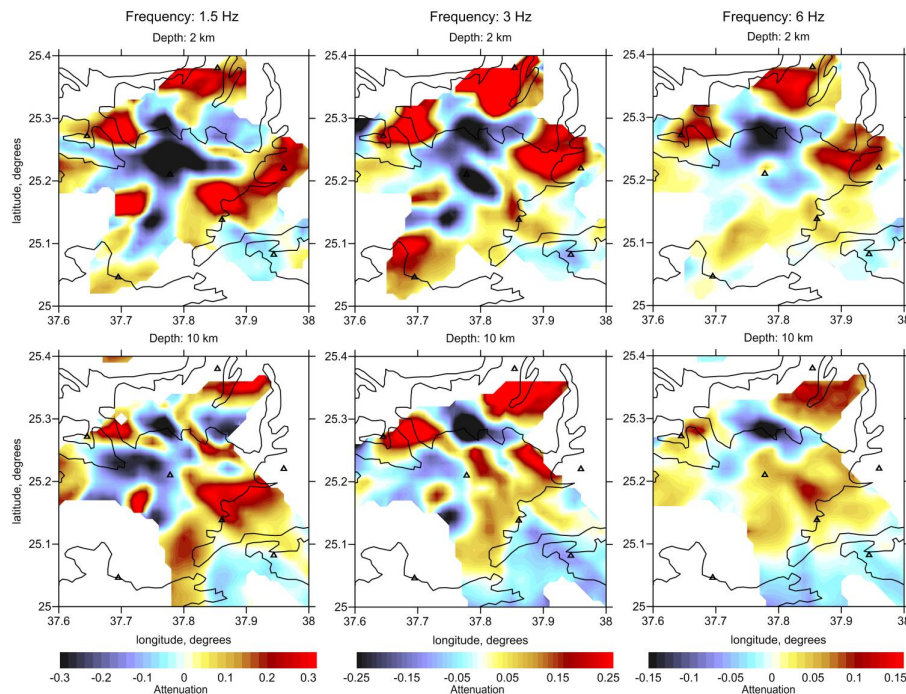


Figure 6. Comparison of the inversion results obtained for the data corresponding to three frequencies: 1.5, 3 and 6 Hz. The results are presented for 2 km and 10 km depth. The triangles are the seismic stations. The black line is the boundary of the basaltic field.

Title Page

Abstract

Introduction

Conclusions

References

Tables

Figures

◀

▶

◀

▶

Back

Close

Full Screen / Esc

Printer-friendly Version

Interactive Discussion



**Attenuation structure
beneath Harrat
Lunayyir**

I. Koulakov et al.

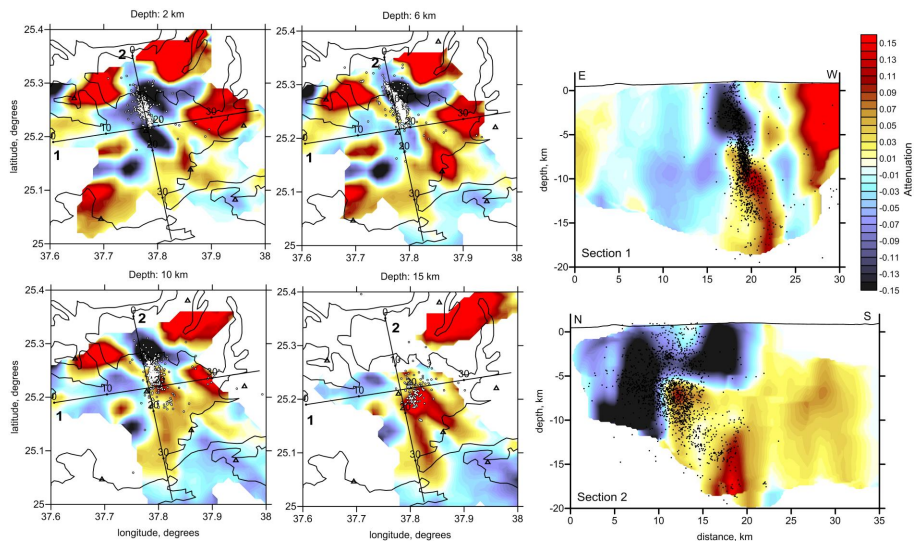


Figure 7. Resulting 3-D distribution of the attenuation in four horizontal and two vertical sections. The dots indicate seismic events near the sections. The triangles are the seismic stations. The black line is the boundary of the basaltic field.

Title Page

Abstract

Introduction

Conclusions

References

Tables

Figures



Back

Close

Full Screen / Esc

Printer-friendly Version

Interactive Discussion

